Design of the intelligent feeding machine for largemouth bass on the basis of feeding intensity

Huang Huang[1,2,3*], Zeyu Zheng[1], Yan Shi[1], Xiao Li[1], Peng Wan[1,2], Zhuo Chen[1], Yunfei Guo[1], He Huang[4]

(1. *College of Engineering, Huazhong Agricultural University, Wuhan 430070, China*;
2. *Key Laboratory of Aquaculture Facility Engineering, Ministry of Agriculture and Rural Affairs, Wuhan 430070, China*;
3. *Key Laboratory of Agricultural Equipment in Mid-Lower Yangtze River, Ministry of Agricultural and Rural Affairs, Wuhan 430070, China*;
4. *Wuhan Mingming Agricultural Technology Co., Ltd., Wuhan 430072, China*)

Abstract: Conventional feeders can achieve timed and quantitative feeding, but they cannot optimize feeding strategies on the basis of actual aquaculture conditions. This study evaluated the feeding intensity of largemouth bass and developed an intelligent feeder to achieve efficient and precise feeding. A mobile feeding system was built by designing and simulating the structure of the data acquisition, control, feeding power, storage, and mobile modules of the feeder. The surface water pressure signals during largemouth bass feeding were collected through pressure sensors and analyzed, and the feeding intensity was classified into three levels: strong, weak, and none. Signal features were extracted to construct a dataset and input into five machine learning models for optimal parameter tuning. The precision, recall, F1 score, and average accuracy of the random forest model were 96.2%, 95.5%, 95.6%, and 93.4%, respectively. The YOLOv5 model was adopted to detect remaining feed on the water surface. The feeding system was designed to enable the feeder to automatically track and provide feed into the tank. Experiments were conducted on the intelligent feeding system, with the feed residue rate as the indicator of the practicality of the feeding system. Verification experiments were also performed on eight tanks, and the average feed residue rate was less than 3%, proving that the feeding system has good practicality in actual aquaculture environments.

Keywords: largemouth bass, feeding intensity, intelligent feeding machine, machine learning, mobile feeding
DOI: 10.25165/j.ijabe.20261902.9955

Citation: Huang H, Zheng Z Y, Shi Y, Li X, Wan P, Chen Z, et al. Design of the intelligent feeding machine for largemouth bass on the basis of feeding intensity. Int J Agric & Biol Eng, 2026; 19(2): 13–27.

1 Introduction

Feeding, as a key step in aquaculture operations, is crucial. At present, most breeding farms in China still rely on manual feeding methods. This method has many drawbacks, including low feeding efficiency, uneven feed distribution, and high feed fragmentation rate, which lead to feed wastage and water pollution[1]. The feeding method in the breeding industry has gradually transitioned from the traditional manual method to the use of automatic feeders to improve production efficiency and expand the breeding scale. Feed casting machines substantially reduce labor costs by feeding feed at regular intervals and in fixed quantities. Atoum et al.[2] designed a fully automated fish feeding system for high-density fish farming environments. This system adopts a two-stage detection mechanism to automatically identify the specific amount of excess feed on the surface of the water tank. However, most conventional feeding machines lack real-time monitoring capabilities for fish behavior and aquatic environment variations, making it impossible to dynamically adjust the feeding plan to achieve optimal feeding effects. Overfeeding not only causes waste of feed, but also reduces the benefit-cost ratio[3]. The accumulation of surplus feed may also lead to water quality deterioration and eutrophication[4]. Insufficient feeding amounts may delay fish growth, cause the body size of the fish population to be uneven, and even stimulate aggressive behavior within the group.

The activity level of fish and the intensity and range of their changes can visually represent the appetite level of fish. The application of machine vision technology in data processing and intelligent feeding can improve production efficiency and reduce breeding costs. This technology promotes the development of aquaculture management towards automation and intelligence[5,6]. The data of fish schools in the feeding state are mainly collected through devices such as cameras and sonar sensors, and the data such as feeding images and sounds in the water are processed and analyzed. When fish conduct feeding behavior, their appetite is evaluated to quantify the hunger level of fish schools[7]. Through in-depth analysis of fish feeding behaviors, feeding management can be optimized to achieve precise control of feed input, thereby effectively reducing feed waste. This method allows aquaculture personnel to adjust the feeding amount and frequency according to the actual needs of fish schools, ensuring the maximization of feed utilization rate and avoiding waste caused by excessive feeding[8]. In actual aquaculture operations, it is particularly important to comprehensively monitor the feeding activities of fish schools and formulate feeding strategies accordingly. Israeli et al.[9] used

Received date: 2025-06-08 **Accepted date:** 2025-12-25
Biographies: Zeyu Zheng, MS, research interest: agricultural mechanization engineering, Email: 13313254370@163.com; **Yan Shi**, MS, research interest: agricultural mechanization engineering, Email: sy14790706679@163.com; **Xiao Li**, MS, research interest: machinery, Email: panoramawindow@163.com; **Peng Wan**, PhD, Professor, research interest: aquaculture equipment, Email: wanpeng09@mail.hzau.edu.cn; **Zhuo Chen**, MS, research interest: machinery, Email: 1284825307@qq.com; **Yunfei Guo**, MS, research interest: machinery, Email: 18239265379@163.com; **He Huang**, MS, research interest: agricultural mechanization engineering, Email: 417587313@qq.com.
***Corresponding author: Huang Huang**, PhD, Associate Professor, research interest: agricultural mechanization and intelligent agricultural management. Huazhong Agricultural University, Wuhan 430070, China Tel: +86-13871571898, Email: huanghuang@mail.hzau.edu.cn.

cameras to calculate the area of projected images of fish schools to evaluate the frequency of fish school jumping behaviors. This method has opened up a new way to analyze the intensity of fish school activities. However, this method can only provide a general and non-specific concept and lacks a numerical representation that can visually show the behavioral intensity of fish schools. Liu et al.[10] used the adaptive Otsu threshold technology and the linear time component identification method to accurately count the remaining feed particles in the water, aiming to reduce the detection error caused by uneven lighting, and successfully controlled the error rate within 8%. This method effectively addresses the challenges under different lighting conditions by intelligently adjusting the threshold, and improves the detection accuracy. Zhang et al.[11] proposed an automatic shrimp counting method using local images and lightweight YOLOv4. The results were consistent with the true values and played a certain role in achieving reasonable feeding and improving breeding efficiency. Li et al.[12] analyzed the local luminance distribution of the image and automatically adjusted the segmentation threshold. This method is not only applicable to the detection of residual feed, but also widely used in other scenarios affected by uneven illumination. Qiao et al.[13] evaluated the intensity of the fish feeding process by analyzing the number of fish schools actively competing for food in the images. However, this method did not track each individual in the fish school, nor did it consider the possible occlusion effect of the water splashes produced by the fish school during the feeding process on the line of sight. The diverse methods for monitoring and evaluating the feeding activities of fish schools using various technologies are gradually maturing. Each method provides insights from different perspectives for understanding the behavior of fish schools. However, the cost of monitoring devices is relatively high, and their application rate in actual aquaculture is low. In order to effectively classify the appetite levels of the perch, the lightweight neural network model MobileNetV3-Small was introduced[14]. With its efficient computing speed and small model size, this model is suitable for rapid and accurate analysis of real-time data, and is particularly suitable for processing the dynamically changing data in the aquaculture scene. Good identification effects have been achieved in complex outdoor breeding environments. Based on several key parameters such as dissolved oxygen saturation, water temperature, and feeding ratio, Zhao et al.[15] adopted a hybrid learning strategy to construct the optimal fuzzy rule base and developed an adaptive fuzzy neural network controller capable of feeding according to real-time demands. Pan et al.[16] analyzed the fluctuations on the surface of the fishpond through a six-axis sensor, collected the state function curves of the feeding behavior of fish schools using this sensor, selected representative characteristic parameters, and further proposed a feeding method according to the feeding habits of fish schools. Du et al.[17] proposed a multimodal fish feeding intensity fusion model in view of the limitations of the single-modal method. They used image stitching technology to fuse these extracted features and processed the fused features through a classifier. The experimental results showed that the accuracy of this model increased by 1.5%-10.8%.

Most of the existing feeding methods based on the feeding activities of fish schools install the data collection devices around the captive tanks. During long-term continuous monitoring, there are high equipment maintenance costs, limited monitoring ranges, and potential hardware failures, making it difficult to guarantee the stability and accuracy of feeding decision-making. When largemouth bass are feeding, the dynamics of water flow change correspondingly due to competition for food or vigorous movements. These changes in water movement can serve as an effective indicator for judging the feeding activity of fish schools. Therefore, this study integrates a mobile chassis into the intelligent feeding system. The mobile chassis navigates to the designated circular culture tank via line-tracking control, and the intelligent feeding system determines the feeding timing and ration based on the aquaculture environment and real-time fish feeding intensity. Based on the above designs, a mobile intelligent feeding system is developed to realize efficient and precise feeding, which is of great significance for improving fish culture efficiency and feed utilization efficiency.

2 Materials and methods

2.1 Experimental location

The experiment was carried out at a land-based industrialized aquaculture base in Xinzhou District, Wuhan City, Hubei Province, China. The experimental facilities included four small-scale aquaculture tanks (diameter of 3.00 m and depth of 1.18 m) and four large-scale aquaculture tanks (diameter of 5 m and depth of 1.8 m). The test subjects were largemouth bass, with about 500 fish in each small tank and 1000 fish in each large tank. All fish were raised in the rearing environment for more than 4 months.

2.2 Overall structure

The Raspberry Pi 4B was used as the upper computer of the feeding system to control the data collection process, manage sensors and external devices, and execute data processing and control tasks. It has a quad-core ARM Cortex-A72 architecture CPU, model Broadcom BCM2711, with a main frequency of 1.5 GHz and 8 GB of RAM. It includes 2 USB 2.0 interfaces, 2 USB 3.0 interfaces, an Ethernet port, an HDMI port, and GPIO pins. The Raspberry Pi 4B runs the Linux-based Raspbian operating system and can implement various data processing software for real-time processing and analysis of collected data. The pressure sensor used in this study was the HM29 digital intelligent pressure transmitter from Nanjing Hongmu Technology Co., Ltd. The core component adopted a 24-bit AD MCU microprocessor with an overall accuracy of 0.05% FS. The image acquisition system includes a Hikvision CCD high-definition camera (model: MV-CS060-10GC) and an MVL-HF0628M-6MPE industrial lens. After assembly, the CCD camera and industrial lens were connected to the Raspberry Pi via a Gigabit Ethernet port and powered by an independent 12 V power supply. The mobile feeding system is composed of five modules: control, data acquisition, feeding power, storage, and mobile modules. The control module comprises the STM32F103ZET6 core control board and the Raspberry Pi 4B. The GPIO pins of Raspberry Pi are connected to the serial pins of STM32, and communication is implemented through the serial port. The data acquisition module is composed of sensors and cameras. The sensor module is connected to an electric push rod with a stroke of 150 mm, and the camera is connected to an electric push rod with a stroke of 600 mm. They are synchronously driven by a lifting platform, which is connected to a ball screw guide rail with a stroke of 900 mm. The feeding power module consists of a Roots blower and a feeder, which serve as the power source for the feeding device. The storage module is a cubic hopper with an inverted conical structure at the bottom and is connected to the discharger. The mobile module employs a four-wheel trolley traveling chassis as the loading platform of the entire device. The structure of the mobile feeding system is shown in Figure 1.

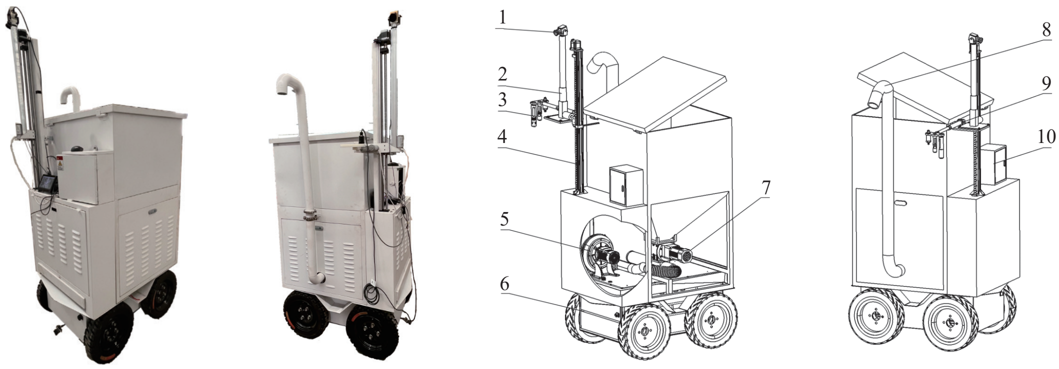

1. CCD imaging module 2. 600-mm-stroke linear electric actuator 3. Multimodal sensor array 4. Ball screw linear guideway 5. Roots blower 6. Four-wheel differential chassis 7. Feed discharge unit 8. Discharge conduit 9. 150-mm-stroke linear actuator 10. Programmable control cabinet

Figure 1 Mobile feeding system

2.3 Design and simulation of the key components of the mobile feeding system

2.3.1 Structural design and simulation of the storage silo

Under normal circumstances, the feed in the silo relies on its own gravity to fall to the feeding device. The efficiency and function of the silo depend on the physical properties of the stored feed and the geometric shape of the silo design. Therefore, in the design process of the storage silo, the volume of the silo and the discharge situation need to be considered to avoid the blockage of the discharge port. After experimental measurement in this study, the feed per 150 cm^3 of space was approximately 51.92 g. The average density of the feed was calculated as follows:

$$\rho = \frac{M}{V} \tag{1}$$

where, M is the feed mass, kg and V is the volume at this mass, m^3.

The calculated average feed density was 346.13 kg/m^3. The breeding environment in this study had a total of eight breeding tanks. The daily feed intake for each breeding tank was approximately 3 kg, the total daily feed intake was 24 kg, and the total feed intake within three days was 72 kg. Therefore, the calculated required feed volume was 0.21 m^3. Considering the existence of gaps when storing granular feed, the actual designed feed storage volume should be larger than the calculated feed volume to ensure sufficient storage space. Therefore, the effective volume of the silo was set to 80% of the designed volume, and the actual volume of the storage silo was 0.27 m^3. Figure 2 shows the overall structure of the storage bin. The storage bin has two parts. The upper part is a 3D quadrilateral structure with a square cross section of 700 mm×700 mm and a height of 500 mm. The lower part is an inverted conical structure with a height of 380 mm. The discharge port is a 55 mm square outlet with a thickness of 2 mm. The storage bin is connected to the chassis through four 710 mm long support columns. The material is 304 stainless steel, which has excellent corrosion resistance, heat resistance, and mechanical properties and is suitable for humid and muggy conditions.

In the design of the silo, the main purpose of adopting the inverted conical structure is to utilize gravity to facilitate the smooth descent of the feed and ensure that the feed can be discharged evenly and continuously. The mechanical relationship between the inner wall of the silo and the granular feed must be analyzed to optimize this structure and determine the size of the discharge port. The forces acting on the falling pellet feed are shown in Figure 3.

The friction coefficient between the inner wall and the pellet feed is a key parameter. Under conditions without lubrication, the friction coefficient is 0.42, and the critical condition is

$$f = mg\sin\alpha = \mu mg\cos\alpha \tag{2}$$

where, f represents the frictional force of the feed on the inner wall; mg is the gravitational force of the feed; μ denotes the friction coefficient of the inner wall surface; and α represents the inclination angle of the inclined plane.

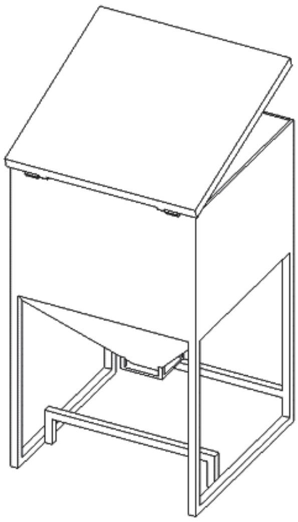

Figure 2 Structure diagram of storage bin

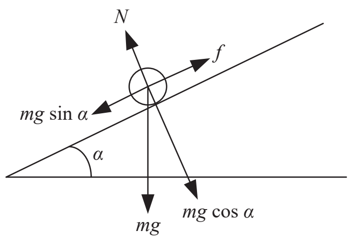

Figure 3 Force diagram of pellet feed falling

The minimum inclination angle of the inclined plane is

$$\alpha = \arctan 0.42 = 22.8^\circ \tag{3}$$

The inclination angle should meet certain requirements in accordance with the empirical equation:

$$\alpha' \geq \alpha + (10^\circ \sim 17^\circ) \tag{4}$$

The angle of the inclined plane α' should satisfy the condition that the component of gravity along the inclined plane is greater than the frictional force. If the angle is set too small, the maximum frictional force will prevent the feed from sliding. Therefore, the inclined angle of the inverted conical structure was designed to be

50° in this study.

If the size of the discharge port is too small, the feed will be blocked. The selected size is calculated with the equation

$$b \geq 6d_1 \tag{5}$$

where, b is the size of the discharge port and d_1 is the equivalent diameter of the pellet feed (i.e., 10 mm).

This study requires a finite element analysis of the static storage silo, so the Abaqus/Standard was used for simulation[18]. The mechanical properties of the material in the silo were edited, Young's modulus was set to 206 000 MPa, and the Poisson's ratio was 0.3. The maximum incremental step number was set to 1000. Load was applied in the silo to simulate the state of loading feed. The contact surface between the silo and the feed was selected as the load application area. The total contact area obtained was 2.2 m^2, and the total weight of the feed was 705.6 N. The applied pressure force was calculated to be 318 Pa, creating the pressure load. Boundary conditions were also set. Given that the bottom of the silo was fixed on the chassis, the contact surface between the bottom and the chassis was set to a completely fixed constraint. The finite element model of the silo was meshed, and the mesh type was selected as tetrahedral mesh with a mesh size of 50 mm. Simulation calculations were performed, and the results are shown in Figure 4.

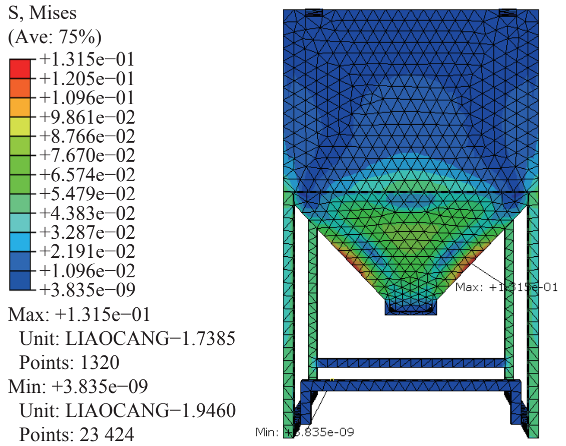

a. Front view

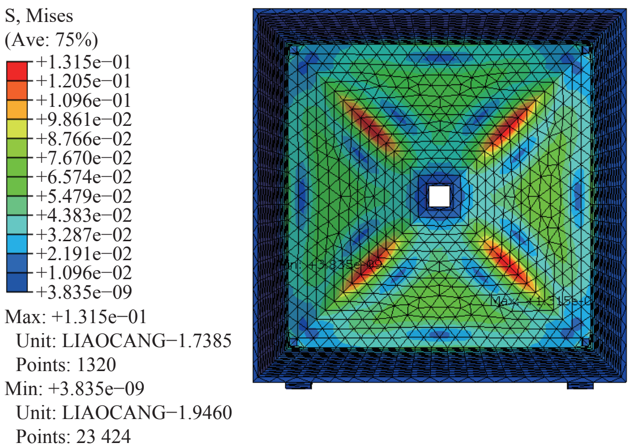

b. Top view

Figure 4 Simulation results of stress in the silo during feed loading process

Figure 4a shows the front view of the storage bin structure. The stress distribution of the model is represented by a color scale diagram, where the stress changes from large to small (from red to blue). Given the extrusion of the feed and the structural design of the silo, the results show that the stress was mainly concentrated in the conical area, and the maximum stress value was 0.135 MPa. Figure 4b presents the internal stress distribution of the storage bin. The load and support conditions formed a uniformly distributed stress field at the bottom. The simulation results indicate that the overall stress of the silo was small, and the structure had not undergone deformation. Therefore, the designed storage silo can be used as the feed transportation device of the feeding system.

2.3.2 Structural design and simulation of conveying pipelines

In consideration of the specific conditions of the test environment, the feeder was installed above the gas-material mixing pipeline, and the Roots blower was used to supply power to convey the feed. The maximum height of the breeding pool was considered 1800 mm, and the height of the chassis carrying the feeding equipment was 540 mm. Therefore, the vertical height of the pipeline must be greater than or equal to 1300 mm. Based on Figure 1, the feeding pipeline of this device is installed on the feeding machine at a height of 100 mm from the chassis. Therefore, the vertical height of the pipeline is set at 1200 mm, the cross-sectional diameter of the pipe was 75 mm, and the inner diameter was 60 mm. The dimension of the upper surface of the chassis was 1055 mm×743 mm. The fan and gas–material mixing pipeline were connected through a 180° hose to make rational use of the space. The angle between the discharge port and the vertical pipe was set to 60° to prevent the feed from being scattered too far. The discharge pipe is shown in Figure 5.

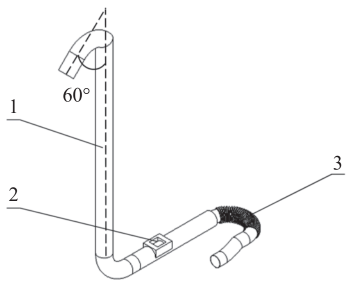

1. Discharge pipe 2. Gas-material mixing pipe 3. 180° hose

Figure 5 Pipeline

Under the working condition of feeding, the interior of the feeding pipeline has the following movement characteristics. The fan is connected to the 180° hose, and the air fluid enters the pipeline. The high-speed flowing air forms the main flow direction in the pipeline, generating substantial airflow dragging force, thereby affecting the movement trajectory of the feed particles. Under the effect of gravity, the feed enters the pipeline. The air flow interacts with the feed particles. Affected by the air flow, the particles change their original falling trajectories and start to accelerate and suspend along the flow direction. In the curved areas at the bottom and top of the vertical pipe, the fluid generates changes in turbulence intensity because of centrifugal force and the inertial effect of the fluid. The feed particles deviate from the center of the airflow and collide with the inner wall of the pipe. As the airflow moves within the pipe, the feed eventually reaches the discharge port along with the air flow.

The feeding pipeline includes 180° hoses, gas–material conveying pipes, and discharge pipes. Given the substantial influence of different performance parameters on the performance of the feeding system, Ansys Fluent software was applied to conduct multiparameter numerical simulation of the abovementioned designed pipeline to explore its airflow performance in the pipeline, assess the movement trajectory of the feed under the influence of the airflow, and verify the inner diameter and height of the pipeline design to determine whether the design is reasonable.

In the numerical simulation of gas–solid two-phase flow in this study, air was set as the main phase, that is, the continuous phase in the gas–solid two-phase flow. Under standard atmospheric pressure, the density was 1.225 kg/m^3, and the dynamic viscosity was 1.7894×10^{-5} kg/m·s. The feed was set as the discrete phase, that is, the discrete solid particles in the gas–solid two-phase flow. The material type was inert particles, and the density was 346.13 kg/m^3.

The established geometric model of the material conveying pipeline was imported into SpaceClaim. In SpaceClaim, volume extraction was used to determine the movement space of the fluid. The model, after volume extraction, was imported into Meshing, and the wall, outlet, and inlet were labeled and defined. Then, the "Generate" option was clicked to generate the mesh. After the grid was imported into Fluent, in the material options, the object parameters of the gas-solid phase were determined, and the boundary conditions were set to simulate the movement states of the gas flow and feed particles in the pipeline.

The main movement characteristics in the pipeline are as follows. The airflow enters the pipeline from the air inlet, and the feed falls into the gas-material mixing pipeline by gravity. Simultaneously, a two-phase flow (gas and solid) is formed and moves to the air outlet. The purpose of the simulation is to observe the interaction between the granular feed and the airflow and the trajectory of the feed in the pipeline, including the behavior of particles falling into the airflow because of gravity and the subsequent movement. Therefore, the discrete phase model (DPM) was employed. This model can simulate the interaction between particles and airflow, such as the influence of drag force and turbulence, thereby predicting the motion state and trajectory of particles accurately. The physical model of DPM uses Saffman lift force.

In DPM, the fluid is regarded as the continuous phase and described using the Eulerian method. The discrete phase describes the dynamic behavior through a series of Lagrange equations[19]. The following text shows the basic principles and equations used to calculate the trajectory of a single particle in DPM. The movement trajectory of particles is governed by Newton's second law.

$$\frac{\mathrm{d}(m_p v_p)}{\mathrm{d}t} = F_D + F_G + F_B + F_L \tag{6}$$

where, m_p is the mass of the particle, kg; v_p is the velocity of the particles, m/s; F_D is the dragging force (N), which is the resistance of the fluid to the particles; F_G is gravity, N; F_B is buoyancy, N; and F_L is the reaction force that the particle experiences due to the pressure gradient and viscous force of the fluid, N.

Dragging force is the most notable force affecting the motion of particles. The calculation equation is as follows:

$$F_D = \frac{1}{2} C_D \rho_f A_p |v_f - v_p| (v_f - v_p) \tag{7}$$

where, C_D is the drag coefficient, which depends on the Reynolds number and the shape of the particles; ρ_f is the density of the fluid, kg/m^3; A_p is the projected area of the particle, m^2; v_f is the velocity of the fluid, m/s; and v_p is the velocity of the particles, m/s.

The geometric model of the material conveying pipeline was established, an independent system of fluid flow (Fluent) was created in Ansys Workbench, the geometric structure was edited, and the geometric model of the material conveying pipeline was imported into SpaceClaim. In SpaceClaim, via volume extraction, the side rings of the cross sections of the air inlet and outlet were selected to determine the movement space of the fluid. The shell of the model was physically suppressed to prevent the remaining geometric features in the computational model from interfering in the fluid simulation.

The model was imported into Fluent. Given that the feed enters the pipe under the action of gravity, gravitational acceleration of 9.81 m/s^2 in the Y direction was defined. In the solver settings, the pressure base was selected as the type, the absolute speed format was selected, and transient was chosen as the time. The pipeline designed in this study had one air inlet, one feed inlet, and one discharge outlet. All boundary conditions were set as velocity inlet conditions. The airflow velocity at the air inlet was set to 25.00 m/s, the feed velocity at the feed inlet was 9.81 m/s^2, and the discrete phase boundary type was selected as "escape," that is, the particles leave the calculation area and do not return.

The SIMPLE algorithm was employed for the iterative solver of pressure-velocity coupling, and the flux type Rhee-Chow was chosen to reduce the numerical oscillation caused by insufficient pressure-velocity coupling.

Figure 6a presents the variation in the static pressure of the pipe from the air inlet to the discharge port. The minimum and maximum pressures were 1128.62 and 9768.76 Pa, respectively, and the pressure variation in the flow area was large. In Figure 6a, the air inlet is shown in red, indicating that the static pressure here is high. The transition from red to blue along the direction of the pipe indicates a gradual decrease in pressure, which is caused by pressure loss due to friction, particle resistance, and backflow when the airflow passes through the pipe. At the air outlet, the static pressure is low because of the accelerated airflow leaving the pipe.

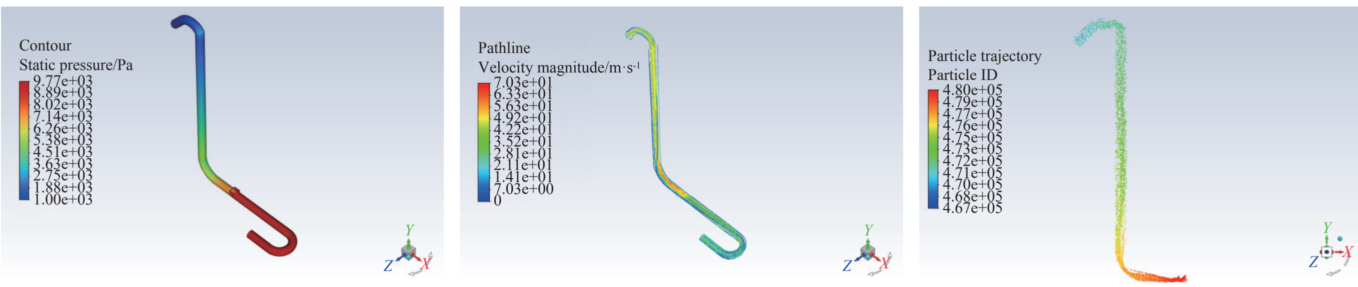

a. Pipeline pressure contour b. Pathline diagram of airflow velocity c. Particle trajectory diagram

Figure 6 Simulation diagram of feed delivery device

The flow velocity distribution inside the pipeline is displayed in a pathline graph. The closer the color is to red, the higher the flow velocity is; the closer the color is to blue, the lower the flow velocity is, as shown in Figure 6b. The air velocity at the air inlet was set to 25.00 m/s. In the middle part between the air inlet and the feed inlet, the air flow velocity was stable, and no obvious backflow or vortex phenomenon occurred. When granular feed was sent to the conveying pipeline from the feeding port, it collided with the airflow moving along the X-axis. Meanwhile, the feed moving along the Y-axis interacted with the airflow, generating vortices inside the pipeline. These vortices formed high-speed airflows in the local areas, which are usually identified as red areas in the image. Because of the effect of the vortex, the particles were drawn into the airflow and conveyed to the discharge port along with the airflow. The minimum and maximum speeds were 3.95 and 47.34 m/s, respectively.

The trajectory of the granular feed in the pipeline was characterized using the particle trajectory diagram, as shown in Figure 6c. Each point in the figure represents the position of the particle at a specific time point, and the different colors represent different particles. The red end in the illustration indicates that the particles are released in a concentrated manner here and have a high density when they enter the pipeline. The granular feed moves along the pipeline with the airflow. The trajectory of the granules begins to disperse because of the unevenness of turbulence, causing the granules to move at different speeds. At the end of the outlet pipe, the particles are spatially dispersed because of the action of varying degrees of fluid force, making their distribution extensive.

The pellet feed was captured at the air outlet. "Trapped" indicates the number of pellets captured. When number tracked= 12 666, trapped=40. As the simulation iteration progresses, number tracked=12 674 means that the new particles have been tracked. At this time, trapped=55 indicates that an additional 15 feed particles have been captured by the air outlet.

In conclusion, when the air inlet velocity is 25 m/s, the pressure parameters and velocity pathlines inside the pipe present good fluid feedback, and the granular feed can be smoothly transported to the discharge port through the airflow. Therefore, when this pipeline design is adopted, the air intake velocity should be ≥25 m/s, and the inner diameter should be 60 mm.

2.3.3 Airflow pressure loss and fan selection

The pressure loss of the airflow in the pipeline mainly includes the friction loss of the wall surface and the local loss of the elbow. The magnitude of the friction loss is positively correlated with the length of the pipeline and is usually calculated using the Darcy-Weisbach equation.

$$\Delta P_f = f_1 \frac{L}{D} \frac{\rho V^2}{2} \tag{8}$$

$$f_1 = 0.0125 + \frac{0.0011}{D} \tag{9}$$

where, ΔP_f is the frictional loss pressure of the airflow in the pipeline, Pa; D is the inner diameter of the pipe, which is 60 mm. The coefficient of friction f_1 can be obtained with Equation (9). L is the length of the pipe, which is 245 cm; ρ is the density of air, kg/m^3; and V is the velocity of the airflow, that is, 25 m/s.

The values are substituted to obtain f_1=0.03, ΔP_f = 468.95 Pa. Both ends of the gas-material mixing pipeline have curved pipes, and the connection between the discharge port and the vertical pipe is also a curved pipe. Local losses occur here, which can be calculated as,

$$\Delta P_1 = \sum \left(K \frac{\rho V^2}{2} \right) \tag{10}$$

where, K is the local loss coefficient, which is taken as 0.17 here.

Local loss pressure $\Delta P_1 = 195.23$ Pa is obtained. For data rationality, a 30% margin is added to achieve $\Delta P_1 = 253.80$ Pa.

Total pressure loss:

$$\Delta P_Z = \Delta P_f + \Delta P_1 \tag{11}$$

where, ΔP_Z = 722.75 Pa. Given that the collision between the feed and the pipe wall during the transportation of the feed can also cause a pressure loss, the margin is increased by 30% to obtain $\Delta P_Z = 939.58$ Pa.

The air volume of a fan is the volume flowing through the cross-sectional area in a unit of time, which can be calculated as:

$$Q = 3600 \frac{\pi D^2}{4} \cdot V \tag{12}$$

The data are substituted into the equation, and Q = 254.47 m^3/h is obtained. The fan parameters selected based on the air inlet velocity and air flow rate are listed in Table 1.

Table 1 Fan parameters

Model	XGB-1500
Platform frame size (length×width×height)/mm^3	350×330×340
Power/kW	1.5
Flow rate/m^3·h^{-1}	263
Rotational speed/r·min^{-1}	2800
Pressure/kPa	34
Weight/kg	23.5
Outlet velocity/m·s^{-1}	≤32

2.3.4 Design of the data acquisition module

The data acquisition module was used to detect changes in water surface pressure and the amount of remaining feed on the water surface. This module is suitable for tanks of different heights, as shown in Figure 7, and can adjust its parameters to adapt to the detection environment. Given that the data of the tanks with heights of 1800 mm needed to be measured in this study, a ball screw guide rail with a stroke of 900 mm was welded to the shell of the feeding trolley. The slider on the guide rail moved vertically through the control of the stepper motor driver and stepper motor. A lifting platform with dimensions of 200 mm×200 mm×10 mm was installed on the slider. It was connected to the platform through two electric push rods with bolts. The 150 mm electric push rod was connected to the sensor module, and the telescopic rod extended along the water surface direction to make the sensor contact the water surface. The 600 mm electric push rod was connected to the CCD camera. The telescopic rod extended vertically, allowing the camera to be at an appropriate height to take pictures of the remaining feed on the water surface.

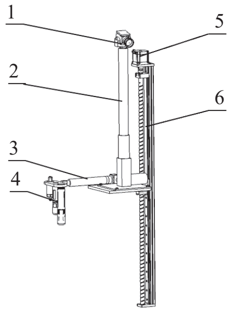

1. CCD camera 2. 600 mm process electric push rod 3. 150 mm process electric push rod 4. Sensor module 5. Stepper motor 6. Ball screw guide rail

Figure 7 Data acquisition module

2.4 Working process

The mobile, intelligent feeding system includes the data acquisition and control module and the chassis auto-tracking module. The data acquisition module is composed of sensors and CCD cameras. The sensors include pressure and water quality sensors, which are used to detect the breeding information in the tank. A CCD camera is used to detect the residual feed on the water surface after each feeding operation, thereby determining whether the feeding process is completed. The data acquisition and control module is used to achieve serial communication between Raspberry Pi 4B and the STM32 development board and to control the electric push rod and ball screw guide rail through the GPIO port. The chassis tracking module detects the navigation trajectory using a linear CCD sensor. The chassis acquires the trajectory image, moves to the designated culture tank, and supports other modules to perform the feeding operation. The overall structural diagram of the system is illustrated in Figure 8.

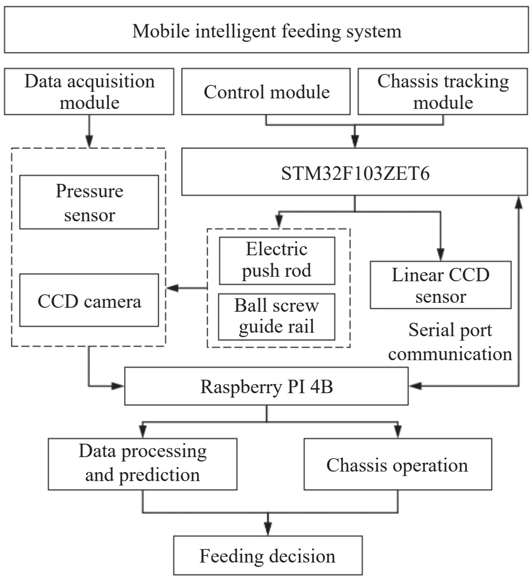

Figure 8 Overall system structure

In accordance with the operation logic of the control system, the feeding operation is realized through the mutual cooperation of the feeding device, the horizontal conveying device, and the data acquisition module. First, the horizontal conveying device moves along the planned path to the designated tank. Through the forward rotation of the stepping motor on the ball screw guide rail, the electric push rod platform is lifted. Second, the transverse electric push rod is controlled to convey the sensor module to the water surface. The longitudinal electric push rod lifts the camera to a certain height. After the sensor and camera receive the data, the data are transmitted to the Raspberry Pi 4B. Third, the data are cleaned and input into the machine learning model to obtain a feeding decision, and precise feeding is implemented accordingly. Finally, the feeding process is completed and the sensors are reset, and the stepping motor of the guide rail is reversed to its initial position. The feeding operation for the current culture tank is completed. This process is repeated to perform feeding operations in the other tanks. The working status of the mobile feeding device is shown in Figure 9.

2.5 Determination of feeding intensity of largemouth bass

2.5.1 Data acquisition method for feeding pressure

During the feeding of largemouth bass, the behavior of snatching food or intense movement can substantially change the dynamics of water flow. The resulting changes in the flow field can be used as an effective indicator to measure the feeding status of fish schools[20]. The variations in these flow fields cause disturbances in the water body, which in turn manifest in the pressure characteristics of the water surface. Therefore, by monitoring the changes in water surface pressure, relevant information about the feeding behavior of fish schools can be indirectly obtained. In this study, the changes in water surface pressure in each round of feeding were measured by immersing pressure sensors below the water surface. The graphs of water surface pressure changes during fish feeding and at the end of feeding are shown in Figure 10.

Figure 9 Working scene of the device

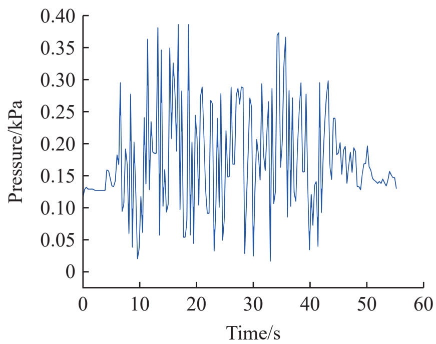

a. Pressure changes on the surface during feeding by fish

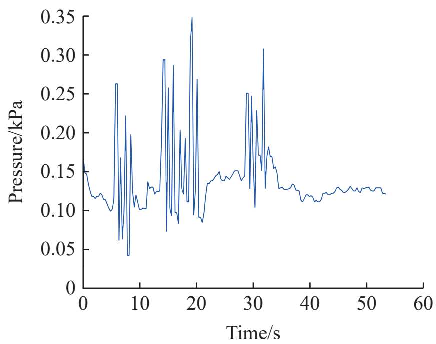

b. Changes in water surface pressure during the end stage of feeding

Figure 10 Curves of changes in water surface pressure during and at the end of fish feeding

When the sensor was immersed 2.5 cm below the water surface, the water surface pressure stabilized at 0.11-0.12 kPa. As indicated in Figure 10a, 0-5 s was the non-feeding stage, and the water surface pressure was between 0.11 and 0.12 kPa. The stage of fish feeding occurred at 5-50 s. At this stage, feeding began. The variation range of water surface pressure was 0.025-0.400 kPa because of the movement, aggregation, and intense reaction of the fish to the feed. Between 50 and 60 s, at the end of this round of feeding, the water surface pressure gradually stabilized. As shown in Figure 10b, drastic changes in pressure occurred during the periods of 5-10, 15-22, and 30-33 s. This result indicates that the fish were at the stage of approaching the end of feeding. The fish did not actively swim toward the feed but consumed the feed in front of them, causing a brief change in pressure until the feeding behavior ended and the pressure value stabilized. In conclusion, the variation in water surface pressure can be used to monitor and predict the feeding intensity of fish schools.

The feeding intensity of fish schools can be classified by analyzing the changes in water surface pressure during the feeding period. In accordance with the classification criteria for the feeding intensity of fish, combined with the collection of pressure under actual experimental conditions, the feeding intensity of fish within 1 min after each round of feeding was classified into three grades: strong, weak, and none[21].

Figure 11 shows the pressure curves of each grade during the feeding of the fish school. The strong grade indicates that the fish are in a state of hunger. This behavioral characteristic shows that the fish have a high demand for feed and exhibit obvious food competition. At this time, the water surface is extremely unstable, with substantial changes in water surface pressure and a long duration. Under these circumstances, after completing the first round of 500 g of feed, another 300 g of feed can be added. The weak grade indicates that some fish in the tank have completed the feeding process, but some unfed fish still consume the feed in front of them. At this time, the water surface fluctuates briefly, with a moderate change in water surface pressure and a short duration. After completing this round of feeding, another 150 g of feed can be added to the tank. The none grade indicates that the fish are in a state of full feeding, showing no obvious reaction to the feed, and the water surface pressure is stable within a certain range. After completing this round of feeding, no further feeding is done.

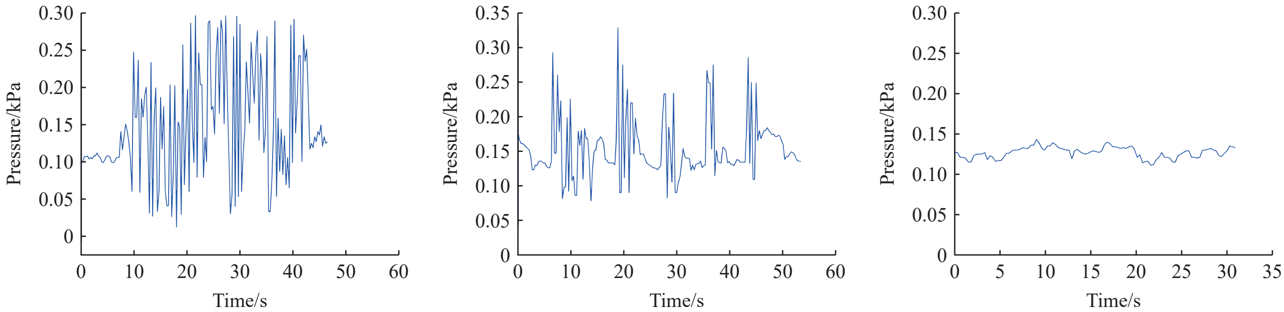

a. Fish schools show obvious stress responses and actively compete for food
b. Fish schools do not actively approach the food but eat the food in front of them
c. The fish have no obvious reaction to the food

Figure 11 Pressure curves for each grade

The sensor data were visualized in real time by using PyQt5 and Matplotlib, and the data were classified using the random forest model. A line graph was created, and the start_plot method was employed to plot the pressure data. Given that the sensor data collection frequency was once every 0.3 s, animation-FuncAnimation was used to set the animation and update the chart once every 0.3 s. The trained random forest model car.pkl was loaded, the calculated feature data were converted into the DataFrame format, and predictions were made using the loaded model. The classification prediction result labels were updated based on the prediction results. The measurement time for each round was set to 1 min. After the measurement was completed, the next step was implemented on the basis of the results on feeding intensity. The pressure acquisition module is shown in Figure 12.

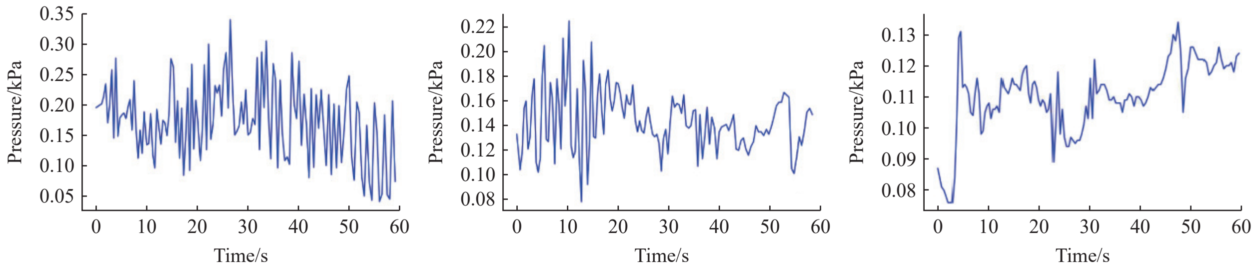

a. Intense hunger
b. Weak hunger
c. Absence of hunger

Figure 12 Pressure measurement module

2.5.2 Selection of pressure signal characteristics

Pressure data were recorded every 0.3 s in the test, and the recording duration for each round was 1 min. Theoretically, each set of data has 200 data points. However, delays occur in data serialization and deserialization during data transmission and processing, resulting in the actual collection of 179 data points for each set of data. A total of 81 sets of data and 14 499 data points were collected. The levels of strong, weak, and none had 27 sets of data each.

Considering that the feeding intensity of fish schools varies substantially at different feeding stages, this study identified and extracted seven key pressure signal characteristics that can reflect the differences. The time-domain characteristics were pressure change frequency, pressure change duration, standard deviation, and mean energy. The statistical characteristics were difference and peak number, and the complexity feature was sample entropy.

The calculation process of the frequency of pressure change is as follows:

Let $P=[p_1, p_2, ..., p_n]$ be a round of pressure measurement values, where n is the total number of measured values, and n =

179. The differences between adjacent measured values are calculated as,

$$\Delta P = [p_2 - p_1, p_3 - p_2, ..., p_{179} - p_{178}] \tag{13}$$

A difference sequence containing 178 elements generates ΔP. The frequency of pressure change, that is, the number of non-zero differences, can be expressed as,

$$f_{\Delta P} = |\Delta p_i| \Delta p_i \neq 0,\ \ \Delta p_i \in \Delta P \tag{14}$$

where, $f_{\Delta P}$ represents the frequency of pressure change and Δp_i is the i-th element in the sequence of differences ΔP.

The calculation of the duration of pressure change is as follows:

1) Set the pressure change threshold to 0.015 kPa. For adjacent measured values, calculate the absolute value of the difference as,

$$\Delta p_i = |p_i - p_{i-1}| \tag{15}$$

2) Determine the positions of Δp_i for the first time and the last time and calculate the duration of the pressure change as,

$$D = i_{end} - i_{start} \tag{16}$$

The calculation of the standard deviation is as follows:

$$\mu_1 = \frac{1}{n}\sum_{i=1}^{n} p_i \tag{17}$$

$$\sigma = \sqrt{\frac{1}{179}\sum_{i=1}^{179}(p_i - \mu)^2} \tag{18}$$

where, p_i represents the i-th measurement value in the pressure data and μ_1 is the average value of all the measured values. Their calculation equations are shown as Equations (17) and (18).

The calculation equation of the mean energy is as follows:

$$E_{\mathrm{m}} = \frac{1}{179}\sum_{i=1}^{179} p_i^2 \tag{19}$$

where, 179 is the number of pressure data points measured per minute.

The pressure difference value is used to measure the difference between the maximum and minimum water pressure in one round of measurement. It reflects the fluctuation range during the fish feeding period and can be used as a direct indicator to evaluate the feeding intensity of fish. The calculation equation is as follows:

$$R = p_{\max} - p_{\min} \tag{20}$$

where, $p_{\max}$ is the maximum pressure value in one round of measurement; $p_{\min}$ is the minimum value of pressure in one round of measurement.

The peak number is the number of times the water pressure signal passes through the threshold line in each round. The threshold of the peak height is set as T = 0.20 kPa, and the calculation equation is as follows:

$$C_T = |\{i | p_i > T, p_i > p_{i-1}, p_i > p_{i+1}, \forall i \in [2, n-1]\}| \tag{21}$$

Let the water pressure data collected in each round be set as $P = [p_1, p_2, ..., p_n]$, where n = 179. Lag parameter m for comparing the vector length of the water pressure signal is defined. Similarity degree r is also defined and set as 0.2 times the standard deviation of the original data. Vector sequence $P_m(i) = [p_i, p_{i+1}, ..., p_{i+m-1}]$of length m is then constructed. For $i = 1, 2, ..., n-m+1$, for each $P_m(i)$, the maximum point-to-point distance from all $P_m(i)$, $i = 1, 2, ..., n-m+1$ is calculated, and the number that satisfies the condition $\max\limits_{k=1,...,m} |p_{i+k-1} - p_{j+k-1}| \leq r$ is counted; this count is called $C_i^m(r)$.

$$C^m(r) = \frac{1}{n-m}\sum_{i-1}^{n-m} C_i^m(r) \tag{22}$$

These steps are repeated to construct vector sequence $P_{m+1}(i)$ with a length of m + 1 and calculate $C^{m+1}(r)$. The sample entropy of the water pressure signal of this round is

$$SampEn = -n\left(\frac{C^{m+1}(r)}{C^m(r)}\right) \tag{23}$$

The feature selection was conducted on the seven initially extracted signal features with the aim of eliminating features that have a low correlation with the recognition of feeding intensity. This could ensure the practicability and effectiveness of the selected feature set and to help simplify the structure of the model and improve its operational efficiency. The XGBoost algorithm was adopted to conduct the feature selection, that is, the calculation of feature importance. XGBoost operates within the gradient boosting framework and employs the additive training strategy. In each iteration step, a new decision tree is introduced to learn the residuals of all previous learners. The gradient boosting process is

$$\hat{y}_i^{(t)} = \hat{y}_i^{(t-1)} + \eta f_t(x_i) \tag{24}$$

where, $\hat{y}_i^{(t)}$ is the predicted value of the model after the t-round iteration, f_t is the decision tree newly added to the model, and η is the learning rate.

The objective function of XGBoost consists of two parts. One is the loss function $L(\theta)$, and the other is the regularization term $\Omega(\theta)$. The regularization term is expressed as,

$$\Omega(f_1) = \gamma T_1 + \frac{1}{2}\lambda\sum_{j=1}^{T} w_j^2 \tag{25}$$

where, f_1 represents a single tree; T_1 is the leaf node tree of the tree; w_j is the score of the j-th leaf node; γ and λ are the regularization parameters.

The objective function of XGBoost is expressed as:

$$Obj(\theta) = \sum_{i=1}^{n} l\left(y_i, \hat{y}_i^{(t)}\right) + \sum_{k=1}^{K}\Omega(f_k) \tag{26}$$

$$Obj(\theta) = \sum_{i=1}^{n} l\left(y_i, \hat{y}_i^{(t)}\right) + \sum_{k=1}^{K}\Omega(f_k)$$

where, $\hat{y}_i^{(t)}$ is the predicted value of the model for the i-th instance; y_i is the corresponding true value; l is the loss function; f_k is the k-th tree; and K is the total number of trees in the model.

The XGBoost model was built, and the dataset containing all the feature attributes was taken as the input for classification training. The model parameters were meticulously adjusted until the optimal classification accuracy was achieved. On this basis, the importance of the features was calculated, and a ranking graph of the importance of the features was generated. The feature importance ranking diagram is shown in Figure 13.

A high score indicates that the feature has a strong ability to distinguish variables for the model. The mean energy and sample entropy characteristics exhibited excellent classification performance in terms of feeding intensity, and the difference, standard deviation, and peak number showed acceptable classification performance in terms of feeding intensity. Meanwhile, the expression ability for change frequency and duration was weak. The use of feature combinations and different model strategies in comparative experiments revealed that retaining the five excellent and good features provided abundant information under specific conditions, thereby improving the overall model performance. The final retained features were mean energy, sample entropy, difference, standard deviation, and peak number. They were adopted as the data sample of the machine learning model to identify the feeding intensity of fish schools. Some characteristic values are listed in Table 2.

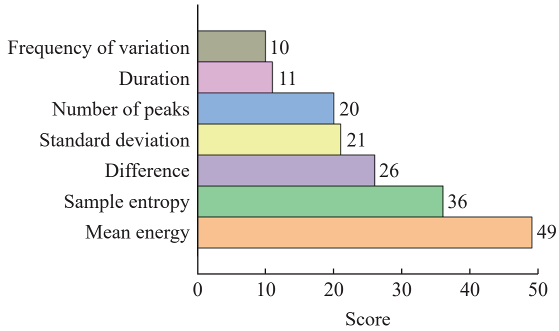

Figure 13 Ranking of feature importance

Table 2 Characteristics and partial characteristic values of five pressure signals

Order no.	Mean energy	Sample entropy	Difference	Standard deviation	Number of peaks	Class label
1	0.039 605 9	−1.364 452 6	0.371	0.086 261 9	38	0
2	0.031 594 7	−2.639 057 3	0.285	0.081 396 7	29	0
3	0.021 387 4	−0.621 688 2	0.303	0.066 544 7	2	1
4	0.020 269 3	−0.810 930 2	0.260	0.051 546 6	2	1
5	0.014 706 3	−0.889 397 9	0.041	0.009 653 1	0	2
6	0.015 855 6	−0.991 192 0	0.034	0.006 657 2	0	2

2.5.3 Selection of data processing models and image acquisition methods

Machine learning, as a core branch in the field of artificial intelligence, occupies an important position in computer science[22]. The application of machine learning in aquaculture has become important in promoting technological progress in the industry and achieving precise aquaculture management. In the feeding management of largemouth bass, the application of machine learning can optimize the feeding strategy. The optimal feed feeding frequency can be accurately calculated by analyzing the feeding intensity of fish schools[23], thereby helping the feeding system make intelligent feeding decisions.

In this study, five traditional machine learning models, namely, decision tree, random forest, gradient boosting, k-nearest neighbor (KNN), and support vector machine (SVM), were selected based on the dataset of the constructed pressure signal characteristics. The feeding intensity of fish schools was identified and analyzed[24-28]. The main function of the image acquisition module was to capture water surface images through a CCD camera and conduct target detection using YOLOv5. In this module, the Software Development Kit (SDK) package of Hikvision cameras was used, and image acquisition was implemented with MvCameraControl_class.

The open_camera function was defined to initialize the camera device, the MV_CC_CreateHandle method was used to create the camera handle, the start_camera method was applied to start the image capture process by using the data buffer of the camera, and the transformation of the camera from the initialization state to image capture was completed. The storage space required for each frame of image data was determined by obtaining the payload (the size of each frame image in bytes), and the buffer was allocated accordingly to prepare for the storage and processing of the image data. A frame of the image data was obtained using SDK, and the data were converted into a NumPy array to create the image.

Next, the detect_objects function was defined to conduct real-time object detection by using YOLOv5, the project path of YOLOv5 was imported, the captured image was taken as a variable pointing to the trained model weight file, a captured frame of the image was preprocessed, and its width was adjusted to 800×600 pixels to reduce the computational load of model processing. The subprocess module in Python was used to call the object detection script, a command string was constructed to call the model execution file detect.py, and the specified weight file best.pt was employed to perform object detection on the temporarily saved image. Given that Raspberry Pi has limited memory for running models, after YOLOv5 had processed the images, the cv2.imshow function of OpenCV was used to display the original images in the window, and the processing results were saved by default in the runs/detect directory of the model project.

3 Results and discussion

3.1 Results and analysis of feeding intensity of largemouth bass

3.1.1 Evaluation of machine learning models

The feeding intensity of fish schools was classified using the machine learning model, and the preprocessed dataset was divided into three categories and inputted into the model. To comprehensively evaluate the performance of different models in identifying the feeding intensity of fish schools, this study employed four key indicators as evaluation criteria; these are average accuracy, precision, recall, and F1 score[29].

Average accuracy is the ratio of all correctly predicted instances to the total number of instances. It can be calculated as:

$$A=\frac{\mathrm{TP}+\mathrm{TN}}{\mathrm{TP}+\mathrm{FP}+\mathrm{TN}+\mathrm{FN}} \tag{27}$$

Precision is the ratio of true positive samples to all samples predicted as positive. The calculation equation is as follows:

$$P=\frac{\mathrm{TP}}{\mathrm{TP}+\mathrm{FP}} \tag{28}$$

Recall measures the proportion of actual positive samples correctly identified by the model, which can be calculated as:

$$R=\frac{\mathrm{TP}}{\mathrm{TP}+\mathrm{FN}} \tag{29}$$

The F1 score is the harmonic mean of precision and recall, providing a balanced measure, which can be calculated as:

$$\mathrm{F1}=\frac{2PR}{P+R} \tag{30}$$

where, TP means true positive (an instance that the model correctly predicts as the positive class), FN stands for false negative (an instance that the model wrongly predicts as a negative class), FP denotes false positive (an instance that the model wrongly predicts as a positive class), and TN stands for true negative (an instance that the model correctly predicts as a negative class).

The constructed dataset of five features and three categories was trained and classified by KNN, SVM, decision tree, gradient boosting, and random forest machine learning models. Table 3 presents the classification effect of the constructed dataset and the various machine learning models compared.

Table 3 Classification results of various models

Model	Precision/ %	Recall/ %	F1 score/ %	Mean accuracy/%
KNN	83.3	82.2	82.5	75.4
SVM	85.0	82.2	82.5	83.1
Decision tree (DT)	89.7	88.9	89.0	90.7
Gradient boosting (GB)	94.7	93.3	93.5	91.0
Random forest (RF)	96.2	95.5	95.6	93.4

Among the five models, KNN and SVM showed low performance because of the influence of the data distribution and neighbor parameter settings. Gradient boosting and random forest are ensemble learning algorithms based on decision trees, so their classification performance in this study was better than that of decision tree. The performance indicators of random forest were slightly higher than those of gradient boosting. Its precision, recall, F1 score, and average accuracy were 96.2%, 95.5%, 95.6%, and 93.4%, respectively, indicating that it has excellent performance in accurately predicting and identifying samples. Moreover, the water surface pressure data may have some noise. Random forest has certain robustness against noisy data and overfitting. Therefore, the random forest model was selected to classify the pressure data and used to guide the feeding decision.

3.1.2 Target detection of remaining feed on the water surface

Object detection algorithms constitute a core research area in computer vision. The main task of object detection algorithms is to identify specific objects in image or video materials and accurately label the categories of these objects and their specific positions in the image. With the advancement and application of deep learning technology, current object detection technologies can be divided into two directions: two-stage and single-stage detection algorithms.

The two-stage object detection algorithms, including region-based convolutional neural network (R-CNN), Fast R-CNN, and Faster R-CNN, generate a series of candidate regions from image data and classify or regression-predict these regions. Two-stage algorithms usually have high accuracy, but because their operation is complex, their processing speed is low. Single-stage object detection algorithms, such as YOLO and single-shot detector, can simplify the detection process by directly performing object classification and bounding box prediction on the image and omit the step of extracting candidate regions. Their advantage lies in their high speed and suitability for application scenarios that require real-time processing[30].

Given the performance of the core processor Raspberry Pi 4B, lightweight YOLOv5 was selected as the model for implementing feed target detection. In the process of object detection, the accuracy and consistency of data are crucial and directly influence the effect of object detection. In view of the complexity of the water surface flow field and the variable detection environment involved, this study created custom datasets that covered the environment under various detection conditions. The purpose of this method is to maximize the diversity and accuracy of the dataset.

The image acquisition camera adopts the Hikvision MV-CS060-10GMGC industrial camera. During the feeding test, the CCD camera was fixed at 1.5 m above the water surface. At the beginning of each round of feeding, because of the fierce feeding behavior of fish schools, a large number of water splashes were produced on the water surface, making the water surface situation extremely complex. This situation increased the difficulty of observing the remaining feed situation. However, as each round of feed release approached its end, the fish's rush for food gradually decreased. At this point, the water splashes and ripples on the water surface correspondingly decreased, and the water surface state became calm, which is convenient for observing and evaluating the remaining feed situation. As shown in Figure 14, when the amount of leftover feed was excessive, block-shaped feed accumulated on the water surface, and the remaining amount of feed could be monitored clearly. The observation results could be used to assess the current feeding desire level of the fish schools accurately.

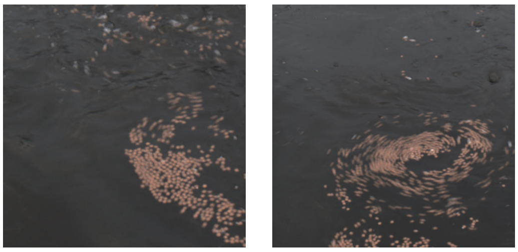

a. Static feed accumulation b. Dynamic feed accumulation

Figure 14 Feed stacking images

During the experimental stage of this study, a total of 2522 images showing the accumulation of feed were collected. By programming, these images were automatically allocated into the training and test sets at a ratio of 8:2. The training set contained 2018 images, and the test set contained 504 images. The LabelImg tool was used for manual annotation to label the feed accumulation in all images and effectively annotate the images. After the annotation work was completed, the annotation information of each image was automatically saved as a corresponding xml file. These files record in detail key information, including the image name, image size, and type and specific location of the target object.

In target monitoring, the indicators for evaluating the performance of algorithms provide key information on the effectiveness of the models. Commonly used evaluation metrics include precision, recall, and mean average precision (mAP). mAP is used to evaluate the overall performance of the model on multiple categories. First, the area AP under the independent precision–recall curve of each category is calculated. This area represents the average performance of the model's precision during the recall change process in that category. Second, mAP is obtained by calculating the average of the AP values of all categories. The specific calculation equation is as follows:

$$\mathrm{AP} = \int_0^1 p(r)\,\mathrm{d}r \tag{31}$$

$$\mathrm{mAP} = \frac{1}{N_1}\sum_{i=1}^{N_1}\mathrm{AP}_i \tag{32}$$

where, $p(r)$ is the precision given the recall r; N_1 is the total number of categories; and AP_i is the AP value of the i-th category.

During mAP calculation, the default intersection over union (IoU) threshold is 0.5, which means the prediction is considered a correct detection only if the IoU of the predicted bounding box is greater than 0.50 compared with the actual bounding box. The mAP value calculated based on this criterion is called mAP@0.5. IoU ranges from 0.50 to 0.95, with a step size of 0.05, and the mAP values under different IoU thresholds are calculated. The final average obtained is called mAP@0.50:0.95. The specific identification results are listed in Table 4. The training results of importing the data into the model are shown in Figure 15.

The YOLOv5 model produced excellent experimental results during training. The model was fast and highly accurate and could run on Raspberry Pi 4B with limited computing resources. Therefore, the YOLOv5 model has good measurement accuracy when it runs on Raspberry Pi 4B. After the training was completed, the generated best model weight file, best.pt, was adopted to evaluate the test part in the self-constructed dataset. The results of this detection process are presented in Figure 16.

The results show that the YOLOv5 model with best.pt weights gives a relatively high confidence score on the test set and has a certain degree of robustness, and it has a good recognition ability for different distributions and densities of feed on the water surface.

Table 4 Experimental data of the YOLO algorithm

Algorithm	Precision/%	Recall/%	mAP@0.5/%	mAP@0.5:0.95/%
YOLOv5	93.3	79.7	93.1	57.9

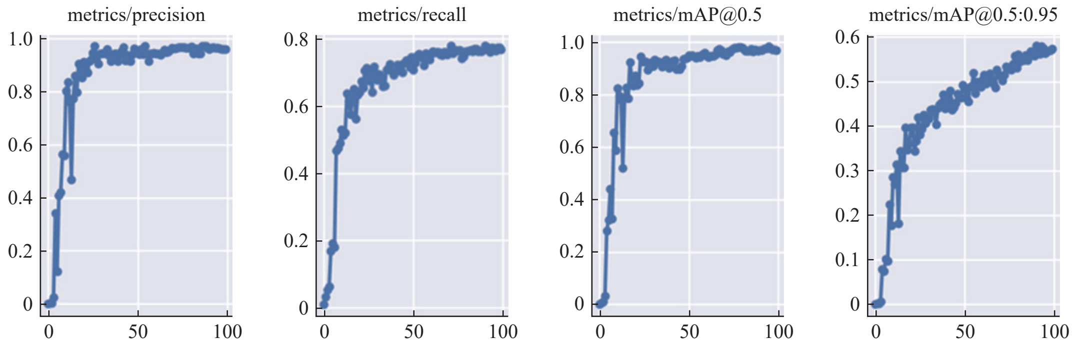

a. Precision b. Recall c. mAP@0.5 d. mAP@0.5:0.95

Figure 15 YOLOv5 training results of feed accumulation images

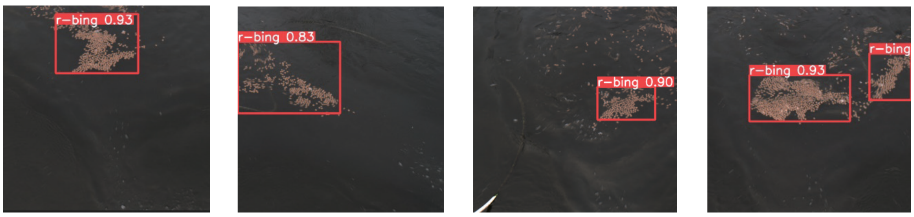

a. R-bing 0.93 b. R-bing 0.83 c. R-bing 0.90 d. R-bing 0.93

Figure 16 Detection results of uneaten feed on water surface

3.2 Test results and verification of the practicability of the mobile feeding system

Two feeding system tests were designed to verify and evaluate the practical performance and effect of the mobile intelligent feeding system. The test environment was indoor culture tanks. Tanks 1-4 were 3 m in diameter and 1 m in water depth; tanks 5-8 were 5 m in diameter and 1.6 m in water depth. The experimental fish were largemouth bass. Approximately 500 fish were placed in the tanks with 3 m diameter, and about 1000 were placed in the tanks with 5 m diameter. All of them had been raised in the breeding environment for more than four months. The fish were assumed to have adapted to the tank environment, minimizing the effect of the breeding environment on the test. An appropriate feeding speed was set through actual feeding scenarios, and the accuracy of the fish school feeding intensity prediction model was tested.

Feeding speed directly affects the uniformity of the feed distribution, the coverage area, and the feeding efficiency of the fish. By calculating the feeding time and speed, the distribution of feed in the water area of the tank can be controlled to make it uniform and reduce the concentrated accumulation of feed. Moreover, by accurately controlling the feeding amount, the breeding cost can be effectively reduced. Therefore, determining the relationship between the feeding speed and the feeding time of the feeding system is essential.

STM32 and the feeding device of the system are connected by two relays to effectively control the feeding device in the intelligent feeding system. The serial port pin of STM32 is connected to the control input terminal of the relay module, and the fan and feeder are connected to the output terminals of the two relays. STM32 outputs a 5 V control signal to the coil of the relay module. The coil generates magnetic force, which makes the contacts close, thereby powering on the 220 V main circuit. When the GPIO port outputs a high level, the relay is energized, and the fan and feeder start. When the GPIO port is at a low level, the relay is disconnected, and the fan and feeder stop working.

In the experiment, No. 5 extruded feed for largemouth bass with a diameter of approximately 6 mm was used. The feeding amounts of the feeding system were measured at five time periods: 0.5, 1.0, 3.0, 5.0, and 10.0 s, and the experiment was repeated five times. At the end of each period, the fed feed was collected and weighed. The feed amounts of the feed systems obtained at different periods are listed in Table 5.

On the basis of data in Table 5, the coefficient of determination (r^2) was introduced as an important indicator for regression analysis to quantify the influence of feeding time on the feeding amount. The range of r^2 is from 0 to 1, which is interpreted as the proportion of the independent variable in the change in the dependent variable. When $r^2 = 1$, the independent variable can fully explain the changes in the dependent variable; $r^2 = 0$ means they are irrelevant.

$$r^2 = 1 - \frac{\sum_i (y_{i1} - \hat{y}_i)^2}{\sum_i (y_{i1} - \bar{y}_i)^2} \tag{33}$$

where, y_{i1} is the actual feeding amount measured in the experiment;

$\hat{y}_i$ is the predicted value of the regression model and $\bar{y}_i$ is the average value of the actual feeding amount.

After calculation, r^2 = 0.9987 was obtained, indicating that a linear relationship existed between feeding time and the output amount. With the data in Table 5, the linear relationship between feeding time and feeding amount was obtained as

$$y = 155.03x - 31.46 \tag{34}$$

where, y represents the expected amount of feed, x is the feed time, and the intercept of 31.46 is the feeding error. The slope indicates that the feeding speed of the feeding system was 155.03 g/s, and the precise feeding of the feeding system was achieved based on this speed.

Table 5 Feed dosage at different times

Time/s	Feed measurement values/g					
	First time	Second time	Third time	Fourth time	Fifth time	Mean value
0.5	64.1	64.8	66.4	63.9	64.5	64.7
1.0	135.3	136.2	135.6	137.4	133.7	135.6
3.0	404.9	406.9	405.3	404.5	407.4	405.8
5.0	726.3	722.1	726.7	728.9	722.9	725.3
10.0	1532.6	1536.2	1533.1	1533.4	1535.5	1534.2

This study adopted the method of multiround feeding in a single field. Specifically, the feeding device used 500 g of feed for a tank in the first round. Then, the system model identified the feeding intensity. If the intensity was judged to be in a state of strong hunger, 300 g of feed was fed in the second round. In the case of weak hunger, 150 g of feed was added. When the fish were no longer hungry and the camera captured the accumulation of feed at this time, the feeding work for this tank was considered completed. The use of multiple rounds of feeding for the same tank in the abovementioned manner aimed to precisely control the distribution of feed, meet the feeding needs of fish at different times, and improve the utilization rate of feed and the efficiency of aquaculture.

After the feeding work in each captive tank was completed, if feed floated on the water surface inside the tank, then the fish were in a state of fullness. At this time, the uneaten feed was collected, dried, and weighed. Aquaculture efficiency and feed utilization efficiency were measured by calculating the feed residue rate.

The uneaten feed needed to be retrieved from the tanks to calculate the feed residue rate, but the retrieved feed had already been soaked in water, which would affect the calculation result. Thus, a vacuum drying oven was used to dry the feed after retrieval. Drying experiments were conducted on feeds with capacities of approximately 150 mL, 250 mL, and 500 mL to verify that the dried feed did not substantially affect the calculation error of the feed residue rate. The masses of the feeds with capacities of 150 mL, 250 mL, and 500 mL were 52.79 g, 90.07 g, and 203.09 g, respectively; after soaking in water, the masses became 63.81 g, 111.53 g, and 242.15 g, respectively, and they were placed in a vacuum drying oven for baking. The temperature of the drying oven was set to 100°C. Given the different amounts and surface areas of the three types of feed, the heating times varied. The drying process was considered complete when the change in feed mass did not exceed 1 g every 30 min.

The water content after drying was determined using the water absorption rate, which provides the proportion of the increment in water absorption relative to the initial mass of dry feed[31]. The water absorption rate of the three types of feed was calculated after drying. The calculation equation is as follows:

$$\mathrm{WUR} = \frac{W_c - W_u}{W_u} \times 100\% \tag{35}$$

where, WUR represents the water absorption rate, W_c is the mass of the dried feed, and W_u is the mass of the feed before soaking.

The water absorption rates of the feed in the three containers were calculated. The water absorption rates of the 150, 250, and 500 mL feed were 2.1%, 3.3%, and 3.9%, respectively.

According to the calculation results, the water absorption rates were all lower than 4%, indicating that the volume expansion and weight increase of the feed in water were not substantial. The weight of the dried feed was approximately equal to the weight of the original dry feed and can thus provide a basis for accurately calculating the feed residue rate.

The objective of the intelligent feeding system is to adjust the amount of feed given on the basis of the real-time hunger demand of fish schools, collect the pressure values during each round of the feeding process, and quantify the hunger degree of fish schools by using the random forest model. Corresponding feeding decisions were made for the three different hunger degrees of strong, weak, and none to maximize the feed utilization rate and improve the overall aquaculture efficiency. Given that the retrieved feed contained the mass of absorbed water, the mass of dried feed was used for calculation to improve the reliability and rationality of the feed residue rate as an assessment indicator of breeding efficiency and feed utilization efficiency. The higher the feed residue rate was, the more excessive the feeding amount was and the poorer the feeding decision was. Conversely, the lower the feed residue rate was, the more accurate the feeding decision was. The calculation equation for the feed residue rate (FRR) is as follows:

$$\mathrm{FRR} = \left(\frac{M_s}{M_a}\right) \times 100\% \tag{36}$$

where, M_s represents the amount of feed that has not been consumed and M_a represents the total amount of feed released during this period.

To ensure the accuracy of the feeding amount data, this study used an intelligent feeding system to conduct a three-day feeding operation on largemouth bass in eight captive tanks. This duration was based on eliminating the influence of contingency on the evaluation of the feed effect, thereby producing stable and reliable data. The results of the feeding test are listed in Table 6.

Table 6 Feed residue rate test results

Tank ID	Item	Day1/g	Day2/g	Day3/g	Average feed residue rate/%
Tank 1	Feed input	800	800	800	0
	Feed residue	0	0	0	
Tank 2	Feed input	650	650	650	0
	Feed residue	0	0	0	
Tank 3	Feed input	650	650	650	0
	Feed residue	0	0	0	
Tank 4	Feed input	800	800	800	0
	Feed residue	0	0	0	
Tank 5	Feed input	1550	1550	1700	2.31
	Feed residue	31.20	26.93	53.94	
Tank 6	Feed input	1700	1850	1850	2.64
	Feed residue	40.41	48.48	54.14	
Tank 7	Feed input	1550	1700	1550	2.68
	Feed residue	44.44	52.10	32.47	
Tank 8	Feed input	1700	1700	1700	2.03
	Feed residue	33.77	31.93	37.61	

The table includes the feeding amount and the remaining amount during the three-day test process. The residue rate of the feed for the three days was calculated, and the average value was obtained. The average residue rate of the feed was less than 3%, indicating the effectiveness of the feeding system in accurately assessing and meeting the actual feeding needs of the fish. Based on aquaculture practices and research, largemouth bass typically cease feeding when the water temperature drops below 10°C. Therefore, this device is programmed to halt feed delivery when the water temperature falls below 10°C to prevent feed waste and maintain water quality. The intelligent feeding decision-making model based on the feeding intensity of fish schools constructed in this study has good practicability. It can improve aquaculture efficiency and the feed utilization rate and has a good application prospect.

4 Conclusions

1) Structural design and simulation analyses were conducted on the mobile feeding system. On the basis of the loading requirements of actual feed quantity, the overall structure of the storage silo was designed, and Abaqus software was applied for stress simulation to verify the strength of the storage silo. A gas–solid two-phase simulation test was performed through Fluent software to determine the air intake velocity of the material conveying pipeline at 25 m/s and the inner diameter of the pipeline at 60 mm. The XGB-1500 model fan was selected as the power source for feeding on the basis of the intake air velocity. The mobile device adopted a four-wheel trolley chassis. The data acquisition module used DC electric push rods and ball screw rails to transport sensors and cameras to the working area.

2) A data acquisition system was built. Raspberry Pi 4B was employed as the upper computer for data acquisition. An HM29 pressure sensor was used to collect water surface pressure data, and a CCD camera was utilized to collect water surface image information. The pressure sensor was connected to Raspberry Pi 4B through the ttyUSB0 serial port, and the CCD camera was connected to Raspberry Pi 4B for communication through the Ethernet port. The feeding intensity of fish schools was quantified through the pressure data, and the pressure data under different feeding states were analyzed. The more intense the feeding of fish schools was, the more obvious the pressure change was. The feeding intensity of the fish schools was classified as strong, weak, and none, and the collected pressure data were divided in accordance with the classification. Then, the feeding rules were specified. After the first round of feeding, when the pressure was judged to be in a strong feeding state, another 300 g of feed was fed in the next round. If it was judged as weak, another 150 g of feed was added. If it was judged as none, no feed was placed. The XGBoost algorithm was used to score each feature. Mean energy, sample entropy, difference, standard deviation, and peak number were retained as the data samples of the machine learning model, and a dataset was constructed.

3) The feed decision-making model was constructed. The dataset was evaluated using five machine learning models, and the optimal parameters were set. The performance indicators of the random forest model were higher than those of the four other models. Its precision, recall, F1 score, and average accuracy were 96.2%, 95.5%, 95.6%, and 93.4%, respectively. Moreover, the random forest model showed certain robustness to noise data and overfitting. Therefore, the random forest model was selected to classify the pressure data and used to guide the feeding decision. The YOLOv5 algorithm was adopted for the target detection of feed, and the dataset was divided into training and test sets at an 8:2 ratio for training. The trained best.pt weight was used to recognize the test set and showed good recognition ability.

4) Practicability verification tests were conducted on the feeding system. The feeding speed of the feeding system was assessed, and the feeding amounts at different periods were recorded to ensure accurate feeding during operation. Using the feed residue rate as the indicator of the practicability of the feeding system, a feed drying test was conducted to improve the authenticity of the feed residue rate. Then, verification tests were performed on eight tanks, and the average feed residue rate obtained was less than 3%. These results demonstrate that the feeding system has good practicability in actual breeding environments.

Acknowledgements

This work was funded by the Fundamental Research Funds for the Central Universities (Grant No. 2662024GXPY005) and Project for R&D, Manufacturing, Promotion, and Application of Agricultural Machinery in Hubei Province (Grant No. 202508).

[References]

[1] Xie L. Analysis on the current situation of industrial recirculating aquaculture. Contemporary Fisheries, 2019; 44(8): 90–91. (in Chinese)

[2] Atoum Y, Srivastava S, Liu X. Automatic feeding control for dense aquaculture fish tanks. IEEE Signal Processing Letters, 2014; 22(8): 1089–1093.

[3] Zhang S M, Li J K, Tang F H, Wu Z, Dai Y, Fan W. Research progress on fish farming monitoring based on deep learning technology. Transactions of the CSAE, 2024; 40(5): 1–13. (in Chinese)

[4] Barraza-Guardado R H, Martínez-Córdova L R, Enríquez-Ocaña L F, Martínez-Porchas M. Effect of shrimp farm effluent on water and sediment quality parameters off the coast of Sonora, Mexico. Ciencias Marinas, 2014; 40(4): 221–235.

[5] Zhou C, Xu D M, Chen L, Zhang S, Sun C H, Yang X T, et al. Evaluation of fish feeding intensity in aquaculture using a convolutional neural network and machine vision. Aquaculture, 2019; 507: 457–465.

[6] Zhang L, Li B, Sun X B, Hong Q Q, Duan Q L. Intelligent fish feeding based on machine vision: A review. Biosystems Engineering, 2023; 231: 133–164.

[7] Sadoul B, Mengues P E, Friggens N C, Prunet P, Colson V. A new method for measuring group behaviours of fish shoals from recorded videos taken in near aquaculture conditions. Aquaculture, 2014; 430: 179–187.

[8] Sneddon L U. Fish behaviour and welfare. Applied Animal Behaviour Science, 2007; 104(3/4): 173–175.

[9] Israeli D, Kimmel E. Monitoring the behavior of hypoxia-stressed *Carassius auratus* using computer vision. Aquacultural Engineering, 1996; 15(6): 433–440.

[10] Liu H Y, Xu L H, Li D W. Detection and recognition of uneaten fish food pellets in aquaculture using image processing. In: Sixth International Conference on Graphic and Image Processing (ICGIP). 2015, Beijing. DOI: 10.1117/12.2179138.

[11] Zhang L, Zhou X H, Li B B, Zhang H X, Duan Q L. Automatic shrimp counting method using local images and lightweight YOLOv4. Biosystems Engineering, 2022; 220: 39–54.

[12] Li D W, Xu L H, Liu H Y. Detection of uneaten fish food pellets in under water images for aquaculture. Aquacultural Engineering, 2017; 78: 85–94.

[13] Qiao F, Zheng D, Hu Y L, Wei Y Y. Research on intelligent feeding system based on real-time decision making of machine vision. Chinese Journal of Engineering Design, 2015; 22(6): 528–533. (in Chinese) DOI: 10.3785/j.issn. 1006-754X.2015.06.003.

[14] Zhu M, Zhang Z F, Huang H, Chen Y Y, Liu Y D, Dong T. Classification of perch ingesting condition using lightweight neural network MobileNetV3-Small. Transactions of the CSAE, 2021; 37(19): 165–172.

[15] Zhao S Q, Ding W M, Zhao S Q, Gu J B. Adaptive neural fuzzy inference system for feeding decision-making of grass carp (*Ctenopharyngodon idellus*) in outdoor intensive culturing ponds. Aquaculture, 2019; 498: 28–36.

[16] Pan S Q, Mao H P, Wang B, Cao H Y, Zhu S Y, Ye Y T. Research on

feeding rules and feeding methods of fish schools based on six-axis sensors. Fishery Modernization, 2023; 50(3): 56–63. (in Chinese) DOI: 10.3969/j.issn.1007-9580.2023.03.007.

[17] Du Z Z, Cui M, Xu X B, Bai Z Z, Han J, Li W C, et al. Harnessing multimodal data fusion to advance accurate identification of fish feeding intensity. Biosystems Engineering, 2024; 246: 135–149.

[18] Shen C L, Zhang L L, Liu H, Wang B Q. Numerical simulation analysis of a strengthening method for shear capacity of a voided slab bridge using finite element software ABAQUS. International Journal of New Developments in Engineering and Society, 2023; 7(2): 070205.

[19] Pavitra S, Pinakeswar M, Pankaj K. Numerical investigation of fluid flow and heat transfer in a gas-solid vortex reactor without slit: Scale-up and optimization. International Communications in Heat and Mass Transfer, 2021; 128: 105590.

[20] Windsor S P, Norris S E, Cameron S M, Mallinson G D, Montgomery J C. The flow fields involved in hydrodynamic imaging by blind Mexican cave fish (*Astyanax fasciatus*). Part II: Gliding parallel to a wall. Journal of Experimental Biology, 2010; 213(22): 3819–3831.

[21] Overli O, Sorensen C, Nilsson G E. Behavioral indicators of stress-coping style in rainbow trout: do males and females react differently to novelty. Physiology& Behavior, 2006; 87(3): 506–512.

[22] Ling J, Heldman D R. Integration of machine learning technologies in food flavor research: Current applications, challenges, and future perspectives. Int J Agric & Biol Eng, 2025; 18(3): 1–11.

[23] Park S, Kim K, Hibino T, Kim K. Machine learning-based prediction of seasonal hypoxia in eutrophic estuary using capacitive potentiometric sensor. Marine Environmental Research, 2024; 196: 106445.

[24] Boutilier J, Michini C, Zhou Z. Optimal multivariate decision trees. Constraints, 2023; 28(4): 549–577.

[25] Reddy D, Murugan R, Nandi A, Goel T. Classification of arrhythmia disease through electrocardiogram signals using sampling vector random forest classifier. Multimedia Tools and Applications, 2022; 82(17): 26797–26827.

[26] Chen Z, Zhang T, Zhang R, Zhu Z M, Yang J, Chen P Y. Extreme gradient boosting model to estimate PM 2.5 concentrations with missing-filled satellite data in China. Atmospheric Environment, 2019; 202: 180–189.

[27] Gary F, Oliver J. On fast computation of finite-time coherent sets using radial basis functions. Chaos (Woodbury, NY), 2015; 25(8): 087409.

[28] Febri L, Agus L H. Adaptive ant colony optimization on mango classification using k-nearest neighbor and support vector machine. Journal of Information Systems Engineering and Business Intelligence, 2017; 3(2): 75–79.

[29] Gopalakrishna A K, Ozcelebi T, Liotta A, Lukkien J J. Relevance as a metric for evaluating machine learning algorithms. Machine Learning and Data Mining in Pattern Recognition: 9th International Conference, MLDM 2013, New York, NY, USA, July 19-25, 2013. Proceedings 9. Springer Berlin Heidelberg, 2013: 195–208. DOI: 10.1007/978-3-642-39712-7_15.

[30] Ho C K, Young S K. Real-time object detection and segmentation technology: an analysis of the YOLO algorithm. JMST Advances, 2023; 5(2-3): 69–76.

[31] Jaisut D, Prachayawarakorn S, Varanyanond W, Tungtrakul P, Soponronnarit S. Accelerated aging of jasmine brown rice by high-temperature fluidization technique. Food Research International, 2009; 42(5-6): 674–681.